Available online at www.sciencedirect.com
ScienceDirect
Advances in Space Research 46 (2010) 58–73
ADVANCES IN SPACE RESEARCH (a COSPAR publication)
www.elsevier.com/locate/asr

Prediction of uncertainties in atmospheric properties measured by radio occultation experiments

Paul Withers

Center for Space Physics, Boston University, 725 Commonwealth Avenue, Boston, MA 02215, USA

Received 3 September 2008; received in revised form 9 November 2009; accepted 4 March 2010

Abstract

Refraction due to gradients in ionospheric electron density, N_e, and neutral number density, n_n, can shift the frequency of radio signals propagating through a planetary atmosphere. Radio occultation experiments measure time series of these frequency shifts, from which N_e and n_n can be determined. Major contributors to uncertainties in frequency shift are phase noise, which is controlled by the Allan Deviation of the experiment, and thermal noise, which is controlled by the signal-to-noise ratio of the experiment. We derive expressions relating uncertainties in atmospheric properties to uncertainties in frequency shift. Uncertainty in N_e is approximately $(4\pi\sigma_{\Delta f} f c m_e \epsilon_0 / V e^2)\sqrt{2\pi H_p / R}$ where $\sigma_{\Delta f}$ is uncertainty in frequency shift, f is the carrier frequency, c is the speed of light, m_e is the electron mass, ϵ_0 is the permittivity of free space, V is speed, e is the elementary charge, H_p is a plasma scale height and R is planetary radius. Uncertainty in n_n is approximately $(\sigma_{\Delta f} c / V f \kappa)\sqrt{H_n / 2\pi R}$ where κ and H_n are the refractive volume and scale height of the neutral atmosphere. Predictions from these expressions are consistent with the uncertainties of the radio occultation experiment on Mars Global Surveyor. These expressions can be used to interpret results from past radio occultation experiments and to perform preliminary design studies of future radio occultation experiments.

Keywords: Radio occultation; Measurement uncertainties; Instrument design

1. Introduction

Radio occultation experiments are commonly used by spacecraft missions to study planetary atmospheres, particularly to measure vertical profiles of both the ionospheric electron density and the number density of neutral gases (Tables 1 and 2). In this paper, the term "atmosphere" is used inclusively to encompass both the "ionosphere" and "neutral atmosphere". The aim of this paper is to derive simple expressions for uncertainties in atmospheric properties that can be used to interpret results from past radio occultation experiments and to perform preliminary design studies of future radio occultation experiments.

The application of radio occultation experiments to planetary science has been described previously by several authors (e.g. Phinney and Anderson, 1968; Fjeldbo et al., 1971; Yakovlev, 2002; Kliore et al., 2004). Sections 2–6 summarize the principles behind radio occultation experiments. They are aimed at readers who may be familiar with the atmospheric measurements made by radio occultation experiments, but who are not familiar with the implementation of such experiments. These sections provide the intellectual foundation required by subsequent sections. Section 7 discusses sources of uncertainties. Section 8 discusses uncertainties for gravity tracking observations. Sections 9 and 10 obtain expressions for uncertainties in atmospheric properties measured by radio occultation experiments. Section 11 summarizes some complications of real radio occultation experiments. Sections 12–14 discuss these results.

2. Planetary radio occultations

Planetary radio occultations depend on the interaction of a radio signal and a planetary atmosphere. In most

E-mail address: withers@bu.edu

0273-1177/$36.00 © 2010 COSPAR. Published by Elsevier Ltd. All rights reserved.
doi:10.1016/j.asr.2010.03.004

Table 1
List of symbols.

Symbol	Meaning	Location of first use
A	Amplitude	Eq. (22)
a	Impact parameter	Section 3
a_j	Value of a for ray path j	Section 3
B	Half of noise bandwidth	Eq. (23)
C	Signal power	Eq. (23)
C_1	A coefficient	Eq. (21)
C_2	A coefficient	Eq. (21)
C_3	A coefficient	Eq. (21)
c	Speed of light	Eq. (3)
e	Elementary charge	Eq. (1)
f	Frequency	Eq. (1)
$f_{measured}$	Measured frequency	Eq. (25)
$f_{nominal}$	Nominal frequency	Eq. (25)
f_p	Plasma frequency	Eq. (2)
f_R	Received frequency	Section 2
f_T	Transmitted frequency	Section 2
G	Gravitational constant	Section 12
H	A scale height	Eq. (28)
H_n	Neutral scale height	Eq. (39)
H_p	Plasma scale height	Eq. (38)
h	A vertical lengthscale	Section 7.1
K_0	A modified Bessel function	Eq. (32)
k_B	Boltzmann's constant	Eq. (16)
L	Distance between tangent point and closest radio element	Section 11
M	Planetary mass	Section 12
m	Mean molecular mass	Section 12
m_e	Electron mass	Eq. (1)
N_0	Noise power density	Eq. (23)
N_e	Electron density	Eq. (1)
n	Label of a sample period	Eq. (24)
n_n	Total neutral number density	Eq. (13)
$n_{n,i}$	Number density of constituent i	Eq. (12)
p	Pressure	Section 5.1
p_s	Standard pressure	Section 5.2
p_W	Partial pressure of water vapour	Eq. (21)
R	Planetary radius	Section 7.1
r	Radius of closest approach of ray path to planetary center	Section 3
r_j	Value of r for ray path j	Section 3
s	Signal	Eq. (22)
T	Temperature	Section 5.1
T_s	Standard temperature	Section 5.2
t	Time	Eq. (22)
V	Speed	Eq. (3)
y	Relative deviation in frequency	Eq. (24)
α	Bending angle	Section 2
α_j	Value of α for ray path j	Section 3
α_{pol}	Molecular polarizability	Section 5.2
β	$\epsilon - 1$	Eq. (15)
ϵ	Relative permittivity or dielectric constant	Section 5.2
ϵ_0	Permittivity of free space	Eq. (1)
η	Complex refractive index	Eq. (1)
θ	Thermal noise	Eq. (22)
κ	Refractive volume	Eq. (13)
κ_i	Refractive volume of constituent i	Eq. (12)
λ	Wavelength	Section 12
μ	Real part of refractive index	Section 3
μ_e	Real part of refractive index of the ionosphere	Section 4
μ_j	Value of μ for ray path j	Section 3
μ_n	Real part of refractive index of the neutral atmosphere	Section 5
ν	Refractivity	Eq. (5)
ν_e	Refractivity of the ionosphere	Section 3
ν_j	Value of ν for ray path j	Section 3
ν_n	Refractivity of the neutral atmosphere	Section 3
ρ	Mass density	Section 5.1
σ_{AD}	Allan Deviation	Eq. (24)
σ_{Ne}	Uncertainty in N_e	Eq. (38)
σ_{nn}	Uncertainty in n_n	Eq. (39)
$\sigma_{thermal}$	Uncertainty in frequency due to thermal noise	Eq. (23)
σ_V	Uncertainty in V	Section 8
$\sigma_{\Delta f}$	Uncertainty in Δf	Eq. (26)
σ_ν	Uncertainty in ν	Eq. (37)
$\tau_{thermal}$	Time interval relevant for thermal noise	Section 7.2
τ_{phase}	Time interval relevant for phase noise	Section 7.3
ϕ	Phase	Section 7.2

cases, geometrical optics provides a sufficiently accurate description of the interaction and the radio signal can be treated as a ray. The propagation of a radio signal through a medium is determined by the medium's complex refractive index. The real part of the refractive index controls phase speed and the imaginary part of the refractive index controls extinction (Eshleman, 1973). Variations in the real part of the refractive index lead to refraction and bending of the ray. The refractive index of a planetary atmosphere is determined by the neutral gases and plasma it contains. As shown in Section 6, it is generally possible to consider contributions to the refractive index from the neutral atmosphere and plasma separately (Eshleman, 1973).

In the case that the effects of magnetic fields and collisions between charged particles and neutrals can be neglected, the complex refractive index of ionospheric plasma, η, is (Rishbeth and Garriott, 1969):

$$\eta^2 = 1 - \frac{N_e e^2}{4\pi^2 m_e \epsilon_0 f^2} \tag{1}$$

where N_e is electron density, e is the elementary charge, m_e is the electron mass, ϵ_0 is the permittivity of free space and f is frequency. Refraction in ionospheric plasma is almost entirely due to electrons, not ions, so only the electron density features in Eq. (1). The total plasma density approximately equals the electron density if the number density of negatively charged ions is much less than the electron density. The plasma frequency, f_p, is defined as:

$$f_p^2 = \frac{N_e e^2}{4\pi^2 m_e \epsilon_0} \tag{2}$$

and the complex refractive index of ionospheric plasma can be expressed as $1 - f_p^2/f^2$. In this case, the real part of the refractive index of ionospheric plasma is always less than unity. If $f > f_p$, then the complex refractive index is real. If $f < f_p$, then the complex refractive index is imaginary.

Table 2
Atmospheres investigated by radio occultation experiments.

Object	Spacecraft
Mercury[a]	Mariner 10
Venus[b]	Mariner 5, Mariner 10, Venera 9, Venera 10, Pioneer Venus Orbiter, Venera 15, Venera 16, Magellan, Venus Express
Earth[c]	GPS/MET, Oersted, CHAMP, IOX, SAC-C, GRACE, COSMIC, Metop-A
Moon[d]	Pioneer 7, Luna 19, Luna 22, SMART-1, SELENE
Mars[e]	Mariner 4, Mariner 6, Mariner 7, Mars 2, Mariner 9, Mars 4, Mars 5, Mars 6, Viking 1, Viking 2, Mars Global Surveyor, Mars Express
Jupiter[f]	Pioneer 10, Pioneer 11, Voyager 1, Voyager 2, Galileo
Io[g]	Pioneer 10, Galileo
Europa[h]	Galileo
Ganymede[i]	Galileo
Callisto[j]	Galileo
Saturn[k]	Pioneer 11, Voyager 1, Voyager 2, Cassini
Titan[l]	Voyager 1, Cassini
Uranus[m]	Voyager 2
Neptune[n]	Voyager 2
Triton[o]	Voyager 2
1P/Halley[p]	Vega 1, Vega 2, Giotto

[a] Fjeldbo et al. (1976).
[b] Yakovlev (2002) and references therein.
[c] Wu et al. (2009) and references therein.
[d] Stern (1999) and references therein; Yakovlev (2002) and references therein; Maccone and Pluchino (2007), Pluchino et al. (2007), Imamura et al. (2008a,b).
[e] Mendillo et al. (2003) and references therein; Pätzold et al. (2005).
[f] Yelle and Miller (2004) and references therein.
[g] Kliore et al. (1975), Hinson et al. (1998a).
[h] Kliore et al. (1997).
[i] Kliore et al. (1998), Kliore (1998).
[j] Kliore et al. (2002).
[k] Gehrels and Matthews (1984) and references therein; Nagy et al. (2006).
[l] Gehrels and Matthews (1984) and references therein; Flasar et al. (2007).
[m] Lindal et al. (1987).
[n] Tyler et al. (1989), Lindal (1992).
[o] Tyler et al. (1989).
[p] Pätzold et al. (1997) and references therein.

Radio signals that propagate from a region of low electron density into a region of high electron density are reflected where $f = f_p$ and never propagate into regions where $f < f_p$. A radio occultation experiment is generally designed such that $f > f_p$. Radar sounders, which probe ionospheres and magnetospheres, are another common type of planetary radio science instrument. They rely on the reflection of radio signals by plasma when $f < f_p$, and hence typically use lower frequencies than radio occultation experiments (Reinisch et al., 2000; Gurnett et al., 2005).

In contrast, the real part of the refractive index of a neutral atmosphere is always greater than unity and neutral atmospheres do not reflect radio signals. Extinction of the radio signal in regions where the imaginary part of the refractive index is large can degrade the quality of the experiment by reducing the signal strength. Critical refraction, defocusing and multipath propagation, which complicate radio occultation experiments, can also occur as a radio signal propagates through an atmosphere. These are discussed in Section 9. The focus of this paper is on the effects of refraction, not extinction. Accordingly, "the real part of the refractive index" is abbreviated to "the refractive index" in the remainder of this paper.

We now introduce some common terms. In planetary science, a radio occultation experiment involves two widely-separated radio elements and a planet. One radio element transmits a radio signal that passes close to the planet under observation before being received by the second radio element. In some cases, the second radio element transmits a radio signal, possibly related to the received signal, back to the first radio element. In other cases, the second radio element functions as a receiver only. The former is called a "two-way" experiment and the latter is called a "one-way" experiment. A two-way experiment requires that both radio elements transmit and receive signals, whereas a one-way experiment does not. A two-way experiment is "coherent" if the second signal is derived directly from the first signal and "non-coherent" if it is not. In a "spacecraft-spacecraft" experiment, each radio element is located on a spacecraft. In a "spacecraft-Earth" experiment, one radio element is located on a spacecraft and the other is located on Earth. An "uplink" signal is transmitted from Earth to a spacecraft and a "downlink" signal is transmitted from a spacecraft to Earth. Note that a single radio element can transmit at one or more frequencies and that the use of multiple frequencies can reduce certain sources of error (Section 7). An "ingress" or "entry" occultation occurs when, from the point of view of one radio element, the other radio element disappears behind the planet. Conversely, an "egress" or "exit" occultation occurs when the other radio element reappears from behind the planet.

There are many possible types of radio occultation experiments. Examples include one-way spacecraft-spacecraft experiments, such as the COSMIC mission (Rocken et al., 2000; Anthes et al., 2008), that use a GPS satellite as the transmitter and a satellite in low-Earth orbit as the receiver; one-way uplink experiments, such as New Horizons (Tyler et al., 2008), that use a ground-based transmitter and a spacecraft receiver; one-way downlink experiments, such as Mars Global Surveyor (Tyler et al., 2001), that use a spacecraft transmitter and a ground-based receiver; and two-way experiments, such as Mars Express (Pätzold et al., 2004), in which a ground-based transceiver uplinks a signal to a spacecraft transceiver, which then downlinks a related signal to the ground-based transceiver.

At any given time, one point along the radio signal's ray path is closer to the center of mass of the planet than any of the other points on the ray path. Depending on the altitude of closest approach, this ray path may pass through the atmosphere of the planet. If so, the ray path is refracted by the atmosphere and it differs from the ray path the

signal would have taken in the absence of refraction. Both the ionosphere and neutral atmosphere contribute to this refraction. Two vectors can be defined, one by the ray path before it entered the atmosphere and one by the ray path after it exited the atmosphere. The "bending angle", α, is defined as the angle between these two vectors (Fjeldbo et al., 1971). This is illustrated in Fig. 1, which shows a one-way downlink experiment at Mars. The frequency received by one radio element, f_R, is not the same as the frequency transmitted by the other radio element, f_T. For instance, the classical Doppler shift expected between two radio elements with a relative speed of 5 km s^{-1} and an X-band frequency of 8.4 GHz is 140 kHz. Refraction of the ray path by the planetary atmosphere introduces an *additional* frequency shift, so the actual received frequency is not identical to the frequency that would have been received in the absence of refraction in the planetary atmosphere. For small bending angles, the magnitude of this frequency difference, Δf, approximately satisfies:

$$\frac{\Delta f}{f} \approx \frac{V\alpha}{c} \tag{3}$$

where V is the relative speed of the two radio elements and c is the speed of light (Hinson et al., 1999, 2000). Eq. (3) neglects some geometrical and other factors; more accurate expressions are given in Appendix A of Fjeldbo et al. (1971) and Eq. (2.2.8) of Kursinski (1997). It is important to note that this approximate relationship should not be used to derive bending angles from measured frequency shifts. For a typical radio occultation experiment in the Martian atmosphere, the maximum value of Δf is about 10 Hz, much smaller than the total Doppler shift (Hinson et al., 1999). Values are larger in denser atmospheres, exceeding 1 kHz at the 1 bar level in the atmospheres of Venus, Jupiter and Titan (Section 13).

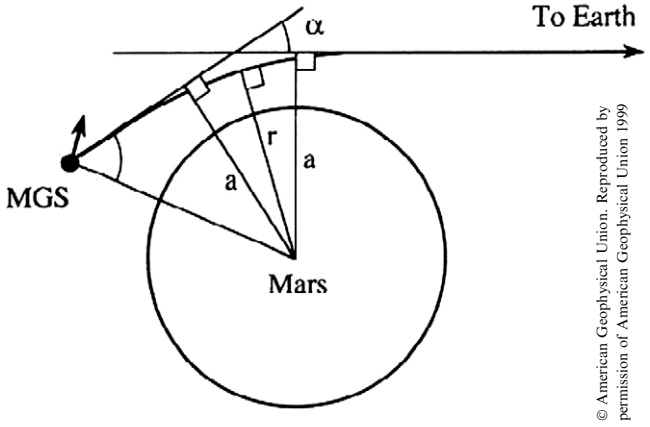

Fig. 1. Schematic illustration of a radio occultation experiment, specifically a one-way downlink experiment conducted at Mars by Mars Global Surveyor (MGS). The bending angle is indicated by α, the impact parameter by a and the radial distance of closest approach by r. Reproduced with minor modifications from Fig. 2 of Hinson et al. (1999). Fig. 2 of Hinson et al., Initial results from radio occultation measurements with Mars Global Surveyor, Journal of Geophysical Research, 104, 26,997–27,012, 1999.

3. Measurement of atmospheric refractivity from bending of ray paths

During an occultation, the received frequency is measured as a function of time. This is then compared to a prediction of the frequency that would have been received in the absence of refraction by the planetary atmosphere to find Δf as a function of time. At each timestep, α can be obtained from Δf, the known spacecraft trajectory and Eq. (3). The impact parameter, a, is defined as the radial distance of closest approach that the ray path would have in the absence of refraction. At each timestep, a can be obtained from the known trajectories of the two radio elements. If the atmosphere's refractive index, μ, is spherically symmetric, then it can be shown that α and a are related by (Fjeldbo et al., 1971):

$$\alpha_j(a_j) = -2a_j \int_{r=r_j}^{r=\infty} \frac{d\ln\mu(r)}{dr} \frac{dr}{\sqrt{(\mu(r)r)^2 - a_j^2}} \tag{4}$$

where r is radius and subscripts indicate a specific ray path, which is usually equivalent to a specific time at the receiver. The radius of closest approach of the ray path whose impact parameter is a_j is r_j. Here we follow Ahmad and Tyler (1998) in adopting the sign convention that positive bending is towards the center of planet, whereas Fjeldbo et al. (1971) used the opposite convention. It is also convenient to define refractivity, ν, which can be positive or negative, as:

$$\nu = \mu - 1 \tag{5}$$

We do not adopt the convention of some other workers who introduce a factor of 10^6 on the left hand side of Eq. (5). Typically, $|\nu| \ll 1$ (Sections 4 and 5). The sign of the bending angle is determined by the sign of $d\ln\mu(r)/dr$, which for weak refraction is the sign of $d\nu/dr$. Ionospheres have negative refractivity and neutral atmospheres have positive refractivity, so radio signals entering an ionosphere from vacuum are refracted in the opposite direction from radio signals entering a neutral atmosphere from vacuum (Section 2). As described by Fjeldbo et al. (1971) and Hinson et al. (1999), Eq. (4) can be inverted to give an expression for μ in terms of α and a:

$$\ln\mu_j = \frac{1}{\pi} \int_{a=a_j}^{a=\infty} \frac{\alpha(a)da}{\sqrt{a^2 - a_j^2}} \tag{6}$$

This inversion is an example of an Abel transform (Phinney and Anderson, 1968; Bracewell, 1986; Ahmad and Tyler, 1998). Eq. (6) can be integrated by parts to eliminate the infinite integrand at $a = a_j$ (Yakovlev, 2002; Pätzold et al., 2004).

$$\ln \mu_j = \frac{-1}{\pi} \int_{a=a_j}^{a=\infty} \ln\left(\frac{a}{a_j} + \sqrt{\left(\frac{a}{a_j}\right)^2 - 1}\right) \frac{d\alpha}{da} da \tag{7}$$

Or equivalently:

$$\ln \mu_j = \frac{-1}{\pi} \int_{a=a_j}^{a=\infty} \cosh^{-1}\left(\frac{a}{a_j}\right) \frac{d\alpha}{da} da \tag{8}$$

After measurements of $\alpha(a)$ are used to determine μ_j, the radial distance to which μ_j corresponds, r_j, must be found. This is accomplished via Snell's law of refraction for spherical geometry, also known as Bouguer's rule, which states that a_j and r_j are related by (Born and Wolf, 1959; Kursinski et al., 2000):

$$\mu_j r_j = a_j \tag{9}$$

Hence $\mu(r)$ can be determined from $\alpha(a)$. The total refractivity of the atmosphere, $v = \mu - 1$, is the sum of the refractivity of the ionosphere, v_e, and the refractivity of the neutral atmosphere, v_n (Eshleman, 1973).

$$v = v_e + v_n \tag{10}$$

In practice, it is possible to determine both v_e and v_n from a single measurement of v for most planetary atmospheres and radio frequencies. This is addressed in Section 6. Vertical profiles of ionospheric electron density and neutral number density can be determined from $v_e(r)$ and $v_n(r)$, respectively, as shown in Sections 4 and 5.

4. Ionospheric refractivity

The relationship between the complex refractive index of an ionospheric plasma and frequency was stated in Eq. (1) for circumstances in which magnetic fields and electron-neutral collisions can be neglected. For typical radio occultation experiments in planetary ionospheres, the real part of the ionospheric refractive index, μ_e, satisfies $|\mu_e - 1| \ll 1$ and, following Eq. (1), μ_e is given by:

$$\mu_e - 1 = v_e = -\frac{N_e e^2}{8\pi^2 m_e \epsilon_0 f^2} \tag{11}$$

Hence $N_e(r)$ can be found from $v_e(r)$. For $N_e = 10^{12}$ m^{-3}, a large electron density for solar system ionospheres, and $f = 8.4$ GHz, $v_e = -6 \times 10^{-7}$, confirming that $|v_e| \ll 1$. Note that ionospheric refractivity is frequency-dependent.

5. Atmospheric refractivity

5.1. Introduction to refractive volume

The refractive index of the neutral atmosphere, μ_n, satisfies:

$$\mu_n - 1 = v_n = \sum \kappa_i n_{n,i} \tag{12}$$

where κ_i is the refractive volume of constituent i and $n_{n,i}$ is the number density of constituent i (Eshleman, 1973). The refractivity of aerosols and condensates, such as dust or clouds, can be neglected because they are transparent at typical radio occultation frequencies. If the chemical composition of the atmosphere is known, then a mean refractive volume, κ, can be defined such that:

$$v_n = \kappa n_n \tag{13}$$

where n_n is the total neutral number density. Hence $n_n(r)$ can be found from $v_n(r)$. For many typical atmospheric gases, κ is on the order of 10^{-29} m^3, similar to their classical molecular volumes (Eshleman, 1973). For a 1 bar atmosphere at 300 K and $\kappa = 10^{-29}$ m^3, $v_n = 2 \times 10^{-4}$, confirming that $|v_n| \ll 1$. The mass density profile, $\rho(r)$, can be found from $n_n(r)$ and the atmospheric composition. The pressure profile, $p(r)$, can be found from $\rho(r)$, the known gravitational field and an upper boundary condition via the equation of hydrostatic equilibrium. The upper boundary condition can be an assumed temperature or pressure. It can also be obtained from the scale height of $n_n(r)$ under certain reasonable assumptions (Withers et al., 2003; Tellmann et al., 2009). The temperature profile, $T(r)$, can be found from $p(r)$, the atmospheric composition and either $n_n(r)$ or $\rho(r)$ via an equation of state, such as the ideal gas law. Errors in the upper boundary condition have minimal effect on the derived pressure and temperature at altitudes more than several scale heights below the upper boundary (Withers et al., 2003). Note that neutral atmospheric refractivity is not frequency-dependent.

5.2. Values of refractive volumes

Refractive volume, which is not typically found in standard reference works, can be related to relative permittivity, ϵ, which is also known as the dielectric constant, and molecular polarizability, α_{pol}. These are commonly found in standard reference works (Lide, 1994).

When the relative permeability (works on electromagnetism frequently use the symbol μ for permeability; this paper does not) of a neutral medium is close to unity, its values of μ_n, the refractive index, and ϵ are related by (e.g. Möller, 1988; Hecht, 2002):

$$\mu_n = \sqrt{\epsilon} \tag{14}$$

Standard reference works, such as Lide (1994), commonly list values of ϵ at standard temperature, T_s, and pressure, p_s. If ϵ can be written as:

$$\epsilon = 1 + \beta \tag{15}$$

where $\beta \ll 1$, then, following Eq. (13) and the ideal gas law, the refractive volume, κ, satisfies:

$$\kappa = \frac{\beta k_B T_s}{2 p_s} \tag{16}$$

where k_B is Boltzmann's constant. The Clausius–Mossotti, or Lorentz–Lorenz, equation, which relates ϵ and α_{pol} can also be used to determine κ (Ashcroft and Mermin, 1964; Robinson, 1973).

$$\frac{\epsilon - 1}{\epsilon + 2} = \frac{4\pi n_n \alpha_{pol}}{3} \quad (17)$$

Eq. (17) assumes that α_{pol} is expressed as a volume (cgs units), not in units of C m^2 V^{-1} (SI units). Use of SI units for α_{pol} requires a factor of $4\pi\epsilon_0$ in the denominator of the right hand side of Eq. (17), where ϵ_0 is the permittivity of free space (Lide, 1994). For $\epsilon - 1 \ll 1$, Eq. (17) can be rearranged to yield:

$$\epsilon = 1 + 4\pi n_n \alpha_{pol} \quad (18)$$

From Eqs. (14) and (18):

$$\mu_n = 1 + 2\pi n_n \alpha_{pol} \quad (19)$$

From Eqs. (13) and (19):

$$\kappa = 2\pi\alpha_{pol} \quad (20)$$

Lide (1994, pp. 6–154) lists relative permittivities at 20 °C (293.15 K) and 101.325 kPa for approximately 40 compounds, including He, Ar, H_2, N_2, O_2, CH_4 and CO_2. Lide (1994, pp. 10–193 to 10–202) also lists polarizabilities of hundreds of compounds, again including He, Ar, H_2, N_2, O_2, CH_4 and CO_2. Refractive volumes derived from relative permittivities and polarizabilities using Eqs. (16) and (20) are the same for these seven species to two significant figures. Values are listed in Table 3. Refractive volumes may also be determined by laboratory measurements (e.g. Essen and Froome, 1951; Essen, 1953; Orcutt and Cole, 1967; Kołos and Wolniewicz, 1967; Tyler and Howard, 1969; Bose and Cole, 1970; Bose et al., 1972).

5.3. Values of atmospheric refractivity

Total refractivity is often represented as the sum of several factors. The following representation is particularly common for the terrestrial atmosphere (e.g. Kursinski et al., 1997; Kursinski, 1997; Tellmann et al., 2009).

$$\nu = C_1 \frac{p}{T} + C_2 \frac{p_W}{T^2} - C_3 \frac{N_e}{f^2} \quad (21)$$

The C_i values are coefficients and p_W is the partial pressure of water vapour. C_1 is κ/k_B, where k_B is Boltzmann's constant (Eq. (13)). C_2 is 0.373 K^2 mbar^{-1} (Kursinski et al., 1997). C_3 is $e^2/(8\pi^2 m_e \epsilon_0)$ (Eq. (11)). Table 4 lists values of C_1 for solar system atmospheres.

Table 3
Refractive volumes, κ, of common atmospheric gases. Values obtained from permittivities and polarizabilities as discussed in Section 5.2.

Species	κ (m^3)
He	1.3×10^{-29}
Ar	1.0×10^{-29}
H_2	5.1×10^{-30}
N_2	1.1×10^{-29}
O_2	1.0×10^{-29}
CH_4	1.6×10^{-29}
CO_2	1.8×10^{-29}

Table 4
Values of C_1 for solar system atmospheres. Tabulated values were found using $C_1 = \kappa/k_B$, values of κ from Table 3 and stated compositions. Compositions are from Lodders and Fegley (1998), with the exception of Titan (Niemann et al., 2005). The abundances of some constituents have been rounded up to ensure that percentages total 100%.

Object	Composition	C_1 (K Pa^{-1})
Venus	96.5% CO_2, 3.5% N_2	1.3×10^{-6}
Earth	78% N_2, 21% O_2, 1% Ar	7.8×10^{-7}
Mars	95.7% CO_2, 2.7% N_2, 1.6% Ar	1.3×10^{-6}
Jupiter	86.4% H_2, 13.6% He	4.5×10^{-7}
Saturn	96.7% H_2, 3.3% He	3.9×10^{-7}
Titan	95.1% N_2, 4.9% CH_4	8.1×10^{-7}
Uranus	82.5% H_2, 15.2% He, 2.3% CH_4	4.7×10^{-7}
Neptune	80% H_2, 19% He, 1% CH_4	4.9×10^{-7}
Triton	100% N_2	8.0×10^{-7}
Pluto	100% N_2	8.0×10^{-7}

6. Separation of atmospheric and ionospheric refractivities

Section 3 showed that ν can be found by a single-frequency radio occultation experiment. Strictly speaking, it is not possible to determine both ν_e and ν_n from a single measurement of ν. However, several properties of ν_e and ν_n make it possible to do so in practice. As shown in Sections 4 and 5, ν_e is always negative and ν_n is always positive. Plasma is much more refractive than neutral gas. For typical frequencies, $|\nu_e|$ is ten orders of magnitude greater than ν_n given identical electron and neutral number densities (Eqs. (11) and (13)). Consider an isothermal neutral atmosphere, loosely based on the Martian atmosphere, that has a surface pressure of 6 mbar, temperature of 200 K, scale height of 8 km and refractive volume of 10^{-29} m^3. Its vertical profile of ν_n, which can be found from Eq. (13), is shown in Fig. 2. Suppose that the ionosphere in this atmosphere is a Chapman layer with its maximum electron density of 2×10^{11} m^3 occurring where the product of the

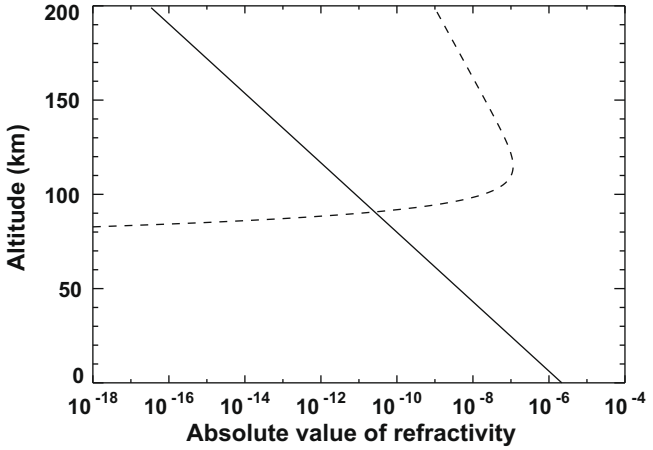

Fig. 2. The solid line shows ν_n and the dashed line shows $-\nu_e$ for the idealized neutral atmosphere and ionosphere discussed in Section 6. Neutral atmospheric refractivity dominates at low altitudes and ionospheric refractivity dominates at high altitudes, with an intermediate region where the magnitudes of both refractivities are extremely small.

absorption cross-section, neutral number density and scale height equals unity (Withers, 2009, and references therein). For a cross-section of 10^{-17} cm^2, the altitude of the ionospheric peak is 115 km. Assuming a frequency of 8.4 GHz, its vertical profile of v_e, which can be found from Eq. (11), is shown in Fig. 2. In the ionosphere, neutral densities are low and electron densities are relatively high, so v_n is very small and v_e is dominant. At lower altitudes, neutral densities are relatively high and electron densities are low, so $|v_e|$ is very small and v_n is dominant. If the uncertainty in refractivity is 10^{-9} (Section 13), then v_n is experimentally indistinguishable from zero above 62 km and v_e is experimentally indistinguishable from zero below 95 km. There is a region spanning four scale heights where both v_n and v_e are experimentally indistinguishable from zero. Similar vertical separations of the contributions of neutral gases and ionospheric plasma occur in other solar system atmospheres.

In practice, the analysis of data from a single-frequency radio occultation uses the following assumptions. If the measured value of v is negative, then v_e is assumed to be identical to the measured value of v and v_n is assumed to be zero; if the measured value of v is positive, then v_e is assumed to be zero and v_n is assumed to be identical to the measured value of v. In the intermediate altitude region below the detectable ionosphere, but above the detectable neutral atmosphere, where v is experimentally indistinguishable from zero, both v_e and v_n are assumed to be zero. Although the two refractivities are not actually zero, they have comparable, but opposite, values in this region. These assumptions are not necessary if v is measured simultaneously at multiple frequencies. Since v_e depends on frequency, but v_n does not, it is straightforward to separate v_e and v_n in such experiments.

7. Sources of uncertainties

7.1. Background

The basic quantities measured in a radio occultation experiment are characteristics of the received radio signal as a function of time. The received frequency is determined as a function of time from these characteristics. Uncertainties in the received frequency during a given time interval result from the finite duration of the time interval, thermal noise and the accuracy of the reference oscillator used as a clock at the receiving radio element. Uncertainties in Δf during a given time interval result from uncertainties in the transmitted frequency, the received frequency, the vacuum Doppler shift between the two radio elements and frequency shifts caused by refraction in plasma in the interplanetary medium (Section 2). If any radio element is on Earth, then frequency shifts caused by refraction in the terrestrial neutral atmosphere and ionosphere are also present. Uncertainties in the vacuum Doppler shift, meaning the Doppler shift that would have been observed in the absence of refraction in the planetary atmosphere under observation, are affected by uncertainties in the trajectories of all spacecraft carrying radio elements and, if any radio element is on Earth, the ephemerides of Earth. Uncertainties in Δf as a function of position result from uncertainties in the ephemerides of the planet being observed, uncertainties in Δf as a function of time, and uncertainties in the trajectories of the radio elements (Section 3). The latter includes uncertainties in the trajectories of all spacecraft carrying radio elements and, if any radio element is on Earth, the ephemerides of Earth. Uncertainties in α as a function of position result from uncertainties in Δf as a function of position, the frequency, the trajectories of the radio elements and c (Section 3). Changes in frequency are usually sufficiently small that it is irrelevant whether the transmitted frequency or received frequency is used in Eq. (3) to find α. Uncertainties in v as a function of position result from uncertainties in α and deviations from spherical symmetry (Section 3). Evaluation of the effects of deviations from perfect spherical symmetry is complicated and beyond the scope of this paper (Ahmad and Tyler, 1999). However, they are not usually considered critical for most applications. The horizontal lengthscale over which this assumption is significant is on the order of $2\sqrt{2hR}$, where h is the vertical lengthscale of the feature of interest, often a scale height, and R is the planetary radius (Kursinski et al., 1997; Hinson et al., 1999; Kursinski et al., 2000). Uncertainties in N_e as a function of position result from uncertainties in v, the frequency, e, m_e and ϵ_0 (Section 4). Changes in frequency are usually sufficiently small that it is irrelevant whether the transmitted frequency or received frequency is used in Eq. (11) to find N_e. Uncertainties in n_n as a function of position result from uncertainties in v and κ (Section 5).

Not all of these uncertainties are equally important for accurate determination of vertical profiles of neutral number density and electron density. The most important are typically those that affect knowledge of Δf. These can be divided into two types: thermal noise and phase noise. If the received signal, $s(t)$, can be described as (Lipa and Tyler, 1979):

$$s(t) = A(t)\sin(2\pi f(t)t) + \theta(t) \tag{22}$$

where t is time, A is amplitude and f is frequency, then phase noise is responsible for variations in f and thermal noise is responsible for θ, which is typically assumed to be normally distributed with zero mean. Variations in A with time are not considered in this paper.

A radio occultation experiment is composed of many parts. This is illustrated in Fig. 3, which shows a one-way downlink experiment conducted by Mars Global Surveyor. Note the reference oscillators on the spacecraft (ultrastable oscillator) and on the ground (frequency timing subsystem), which contribute to the phase noise, and the many parts through which the radio signal passes, which contribute to the thermal noise.

7.2. Thermal noise

The uncertainty in frequency due to thermal noise, $\sigma_{thermal}$, is (Simon and Yuen, 1983; Lindsey, 1972):

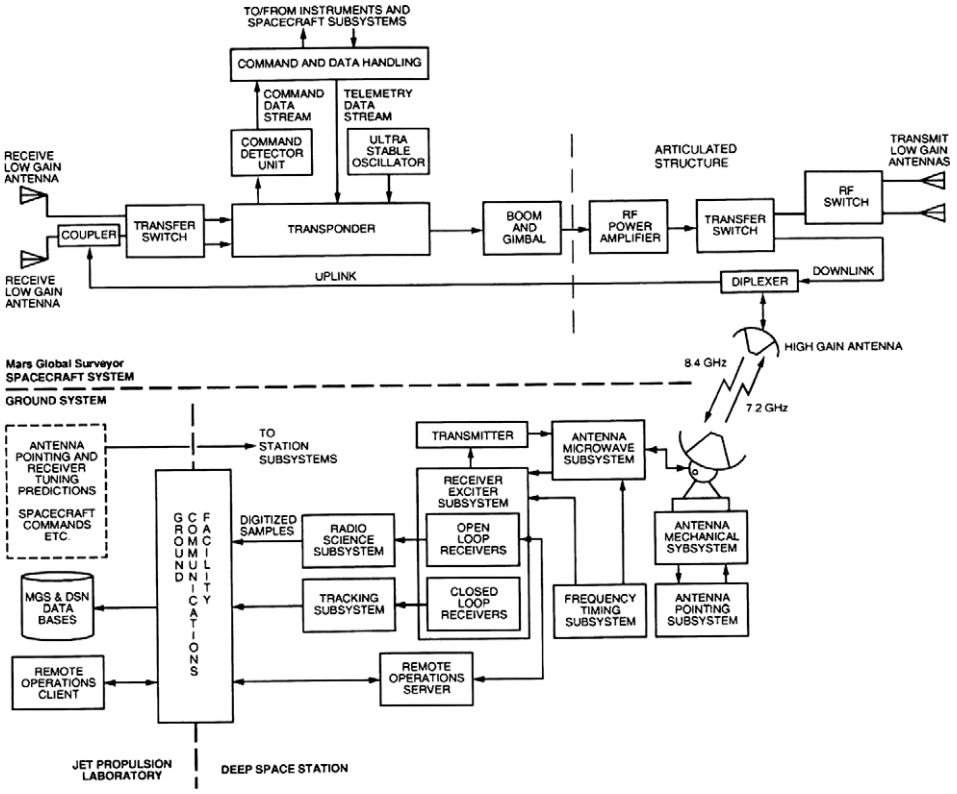

Fig. 3. Block diagram of a radio occultation experiment, specifically a one-way downlink experiment conducted at Mars by Mars Global Surveyor. Reproduced from Fig. 7 of Tyler et al. (2001). Fig. 7 of Tyler et al., Radio science observations with Mars Global Surveyor: Orbit insertion through one Mars year in mapping orbit, Journal of Geophysical Research, 106, 22,327–23,348, 2001.

$$\sigma_{thermal} = \frac{\sqrt{2BN_0/C}}{2\pi\tau_{thermal}} \tag{23}$$

where $2B$ is the noise bandwidth (Hz), N_0 is the noise power density (W Hz^{-1}), C is the signal power (W) and $\tau_{thermal}$ is the time interval for this measurement (seconds).

A qualitative justification for this expression is as follows. The signal amplitude can be represented as $A\sin\phi + \theta$, where ϕ is phase. An experimenter examining a time series of amplitudes can only be confident that one cycle has ended and another begun when $A\sin\phi > \theta$. For small values of θ/A, this leads to an uncertainty in phase at any time of θ/A. Since amplitude is proportional to the square root of power, this is equivalent to the reciprocal of the square root of the signal-to-noise ratio or $\sqrt{2BN_0/C}$. The uncertainty in the number of cycles in this time series is $1/2\pi$ times this or $(\sqrt{2BN_0/C})/(2\pi)$. The uncertainty in the frequency of this time series is the ratio of this to the duration of the time series or $(\sqrt{2BN_0/C})/(2\pi\tau_{thermal})$, as stated in Eq. (23).

A representative value for C/N_0 is 50 dB Hz or 10^5 Hz (Nagy et al., 2006). A representative value for B is 100 Hz (Hinson et al., 1998b). A representative value of $\tau_{thermal}$ is 1 s (Hinson et al., 1999). From Eq. (23), a representative value of $\sigma_{thermal}$ is 10 mHz, consistent with the value reported in Hinson et al. (1999). Thermal noise is produced at all stages of the experiment, including each transmitter and receiver.

7.3. Phase noise

There are many sources of phase noise, including instabilities of all reference oscillators used in the experiment and variations in refractive index in the terrestrial atmosphere, terrestrial ionosphere and plasma in the interplanetary medium. If an oscillator's output frequency is extremely stable, then it is called an "ultrastable oscillator" or USO. This label is often applied to space-based oscillators. In a one-way experiment, instabilities of the reference oscillators at both the transmitter and receiver contribute to the phase noise. The reference oscillator at the transmitter affects the stability of the transmitted frequency. The reference oscillator at the receiver affects the accuracy with which the received frequency can be measured. The received frequency cannot be measured to one part in a billion if the clock at the receiver is only stable to one part in a thousand, for example. In a two-way coherent experiment, the most stable radio element can be used as the transmitter. The least stable radio element can receive the signal, then transmit a signal that is coherently related to the received signal. In this case, the stability of the signal transmitted by the least stable radio element and received at the end of the experiment is unaffected by the frequency stability of the least stable radio element. Despite eliminating one source of phase noise, two-way coherent experiments are not always better than one-way experiments. The time required to establish the two-way coherent

link at the onset of an egress occultation results in loss of data at low altitudes. Two-way coherent links are also difficult to maintain when the signal passes through a dense atmosphere, such as the atmosphere of Venus or Jupiter, and its amplitude varies dynamically.

Refraction along the ray path from regions other than the atmosphere of the planet under observation are sources of phase noise. Refraction due to plasma in the interplanetary medium is always a source of phase noise. For a radio occultation in which one radio element is ground-based, refraction in the terrestrial neutral atmosphere and ionosphere also contributes to the phase noise. A baseline correction for these effects can be made using signals recorded when the ray path is far from being occulted by the planet under observation and is not refracted at all by its atmosphere, but the actual contribution of these effects will inevitably vary somewhat about the baseline. Spatial variations in the terrestrial neutral atmosphere and ionosphere are not typically a concern, since the location in the sky of the space-based radio element does not change significantly over the duration of the experiment, typically on the order of minutes.

Turbulence in interplanetary plasma (that is, the solar corona and solar wind) is often the most significant source of undesirable refraction (Sniffin, 2001). Large interplanetary plasma densities are not in themselves a major problem as the effects of homogeneous plasma can be removed by baseline corrections. Variations in the column density of interplanetary plasma along the ray path due to true temporal variations or motion of the ray path through spatially varying regions of plasma can produce phase noise. In addition, plasma inhomogeneities on a scale small by comparison with the signal's Fresnel zone can produce phase noise as the assumptions of geometrical optics are violated. The relevant length scale is the square root of the product of the wavelength and the distance between the inhomogeneous region and the closest radio element. This length scale is on the order of 100 km for wavelengths of a few centimetres and a separation of 1 AU. Variations in antenna pointing can also be a source of phase noise.

The phase noise is characterized by the Allan Deviation, σ_{AD}, which is defined as (Allan, 1966):

$$\sigma_{AD}^2 = \frac{1}{2}\left(y_{n+1} - y_n\right)^2 \tag{24}$$

where angle brackets indicate the expectation value of the enclosed quantity, y_n is the value of y from the nth sample period and y is given by:

$$y = \frac{f_{measured} - f_{nominal}}{f_{nominal}} \tag{25}$$

The frequency $f_{measured}$ is the measured frequency over a sample period or integration time of duration τ_{phase}. If $f_{measured}$ comes from a normal distribution with mean $f_{nominal}$, then $\sigma_{AD} f_{nominal}$ equals the standard deviation of the normal distribution. However, although $\sigma_{AD} f_{nominal}$ is often treated as if it were a standard deviation, it is not formally identical to a standard deviation. The Allan Deviation is a function of the integration time, τ_{phase}.

The phase noise in the complete radio occultation experiment is characterized by an Allan Deviation. In addition, the contribution to the phase noise from an individual component within the complete experiment can be characterized by an Allan Deviation. Typical values of Allan Deviations for space-based oscillators on the 1–1000 s timescales that are relevant for radio occultations are on the order of 10^{-13} (Tyler et al., 2001; Kliore et al., 2004). Equivalent values for ground-based oscillators at the NASA Deep Space Network are on the order of 10^{-14} to 10^{-15} (Dick and Wang, 1991; Howard et al., 1992; Thornton and Border, 2003; Asmar et al., 2004).

In a typical two-way coherent radio occultation experiment, the signal is unaffected by the Allan Deviation of the space-based oscillator. The Allan Deviation of the complete radio occultation experiment must be no smaller than the Allan Deviation of each reference oscillator that is used in the two radio elements. In practice, σ_{AD} exceeds this lower limit due to the other sources of phase noise, particularly variations in interplanetary plasma density along the ray path for single-frequency radio occultation experiments.

7.4. Implications

The duration of radio occultation experiments is typically set so that some of the measurements are made when the ray path is far above the atmosphere of the planet being observed and unaffected by refraction in this atmosphere. These unaffected measurements provide a baseline from which thermal noise, phase noise and, for a one-way downlink experiment, transmitted frequency can be determined. The frequency produced by a space-based oscillator drifts with time, so its frequency is not identical to the frequency determined during pre-flight testing.

The uncertainty in Δf, $\sigma_{\Delta f}$, depends on $\sigma_{thermal}$ and $\sigma_{AD} f$ in the usual manner:

$$\sigma_{\Delta f}^2 = \sigma_{thermal}^2 + \sigma_{AD}^2 f^2 \tag{26}$$

If $\sigma_{AD} = 3 \times 10^{-13}$ and $f = 8.4$ GHz, then $\sigma_{AD} f$ equals 3 mHz, less than the representative value of $\sigma_{thermal}$ of 10 mHz. Uncertainties in radio occultation experiments are not solely determined by the Allan Deviations of reference oscillators. For example, the uncertainties in radio occultation experiments performed by the Galileo orbiter significantly exceeded those anticipated during mission design because the signal power was lower than planned. This occurred despite the excellent in-flight Allan Deviation of the onboard oscillator. Signals had to be transmitted through Galileo's low gain antenna because the high gain antenna failed to deploy (Howard et al., 1992; Hinson et al., 1997).

8. Velocity uncertainties for gravitational studies

If radio tracking is used to measure the speed of one radio element with respect to the other radio element, as in gravitational studies (e.g. Rappaport et al., 1997), then

the uncertainty in speed, σ_V, is simply the product of c/f and the uncertainty in frequency shift. This is valid for a one-way experiment. For a two-way coherent experiment, c/f is replaced by $c/2f$ because the signal is Doppler-shifted on both legs of its journey.

The observed value of $\sigma_{\Delta f}$ is typically smaller during a gravity tracking flyby than during an occultation because the timescale for frequency changes is much longer during a gravity tracking flyby than during an occultation (e.g. Rappaport et al., 1997; Hinson et al., 1999). This permits longer $\tau_{thermal}$, which reduces $\sigma_{thermal}$, and longer τ_{phase}. The Allan Deviations of reference oscillators generally decrease as the integration time τ_{phase} increases from seconds to thousands of seconds. (Howard et al., 1992; Tyler et al., 2001; Kliore et al., 2004). For example, the Allan Deviation of the oscillator on the Galileo Orbiter was 3×10^{-11}, 4×10^{-12}, 1×10^{-12} and 1×10^{-12} for integration times of 1, 10, 100 and 1000 s (Howard et al., 1992). For a one-way experiment in which thermal noise is dominant, σ_V satisfies:

$$\sigma_V = \frac{c\sqrt{2BN_0/C}}{2\pi f \tau_{thermal}} \tag{27}$$

This value is halved for a two-way coherent experiment (Pätzold et al., 2004).

9. Relationship between bending angle and refractivity

In order to relate uncertainties in N_e and n to uncertainties in Δf, we must simplify the Abel transform relationship between the bending angle, α, and the refractivity, v (Eq. (4)).

The bending angle, α, is a function of the shape of the vertical refractivity profile. For neutral atmospheres or the topsides of ionospheres above their main peaks, it is often reasonable to assume that refractivity, v, which is proportional to electron density or neutral number density, decreases exponentially with increasing altitude. An ionosphere controlled by diffusion will have an exponential vertical profile, as will the topside of a Chapman-like ionosphere (Rishbeth and Garriott, 1969; Schunk and Nagy, 2000; Withers, 2009).

$$v(r) = v_j \exp\left(\frac{-(r - r_j)}{H}\right) \tag{28}$$

where v_j is the refractivity at radius r_j and H is a scale height. Using Eq. (5) that defines v as $\mu - 1$, $d\ln\mu/dr$ satisfies:

$$\frac{d\ln\mu}{dr} = \frac{-v_j}{H}\exp\left(\frac{-(r - r_j)}{H}\right) \tag{29}$$

Eq. (4) becomes:

$$\alpha_j = \frac{2a_j v_j}{H}\int_{r=r_j}^{r=\infty} \exp\left(\frac{-(r - r_j)}{H}\right)\frac{dr}{\sqrt{(\mu(r)r)^2 - a_j^2}} \tag{30}$$

For neutral pressures less than hundreds of bars and for all planetary ionospheres, $|v_j| \ll 1$ as shown in Sections 4 and 5. Hence r_j can be replaced by a_j (Eq. (9)) and μr can be replaced by r (Eq. (5)) to give:

$$\alpha_j = \frac{2a_j v_j}{H}\int_{r=a_j}^{r=\infty} \exp\left(\frac{-(r - a_j)}{H}\right)\frac{dr}{\sqrt{r^2 - a_j^2}} \tag{31}$$

The solution of Eq. (31) is (Arfken and Weber, 1995, Eq. (11.122)):

$$\alpha_j = \frac{2a_j v_j}{H}\cdot\exp\left(\frac{a_j}{H}\right)\cdot K_0\left(\frac{a_j}{H}\right) \tag{32}$$

where $K_0(a_j/H)$ is the modified Bessel function of the second kind of order 0. Since a_j is on the order of the planetary radius, $a_j/H \gg 1$. In this limit (Arfken and Weber, 1995, Eq. (11.127)):

$$K_0\left(\frac{a_j}{H}\right) \to \sqrt{\frac{\pi H}{2a_j}}\cdot\exp\left(\frac{-a_j}{H}\right) \tag{33}$$

Therefore:

$$\alpha_j = v_j\sqrt{\frac{2\pi a_j}{H}} \tag{34}$$

$$\alpha(a) = v(r)\sqrt{\frac{2\pi a}{H}} \tag{35}$$

A similar result is stated in Eshleman et al. (1979) and Yakovlev (2002). As long as the refractivity increases exponentially as altitude decreases, the bending angle also increases exponentially as altitude decreases.

From Eqs. (3) and (34), the expected frequency shift, Δf, satisfies:

$$\Delta f(a) \approx \frac{fVv(r)}{c}\sqrt{\frac{2\pi a}{H}} \tag{36}$$

Recall that this is an approximation since the assumed relationship between frequency shift and velocity is approximate. In particular, Eq. (3) is only a realistic approximation for small bending angles. It is important to note that this relationship should not be used to derive refractivity profiles from measured frequency shifts. Eq. (36) remains approximately true if the assumption of an exponential dependence of refractivity on altitude is invalid, as long as $v(r)$ decreases with increasing altitude with characteristic lengthscale H.

10. Expressions for uncertainties in electron density and neutral number density

The vertical extent of most planetary atmospheres and ionospheres is much smaller than the planetary radius, R, although Titan and comets are exceptions. Hence we substitute R for a in Eq. (36). From Eq. (36), the uncertainty in refractivity, σ_v, is related to $\sigma_{\Delta f}$ via:

$$\sigma_v \approx \frac{c\sigma_{\Delta f}}{Vf}\sqrt{\frac{H}{2\pi R}} \tag{37}$$

If the refractivity from Eq. (11) is equated to σ_v in Eq. (37), and the resultant equation is rearranged, then the uncertainty in electron density, σ_{Ne}, satisfies:

$$\sigma_{Ne} \approx \frac{4\pi\sigma_{\Delta f} f c m_e \epsilon_0}{Ve^2}\sqrt{\frac{2\pi H_p}{R}} \tag{38}$$

where H_p is the scale height of ionospheric plasma, which is not necessarily identical to the neutral scale height at ionospheric altitudes. If the refractivity from Eq. (13) is equated to σ_v in Eq. (37), and the resultant equation is rearranged, then the uncertainty in neutral number density, σ_{nn}, satisfies:

$$\sigma_{nn} \approx \frac{c\sigma_{\Delta f}}{Vf\kappa}\sqrt{\frac{H_n}{2\pi R}} \tag{39}$$

where H_n is the scale height of the neutral atmosphere. We do not consider errors in pressure and temperature in this paper, which are derived from a vertical integration of the neutral number density, except to note that their relative errors decrease as altitude decreases (Hinson et al., 1999).

Again, it is important to note that these relationships should not be used to derive neutral number density or ionospheric electron density profiles from measured frequency shifts. We assert without proof that these relationships remain valid when the refractivity does not vary exponentially with altitude, such as around an ionospheric peak. Published uncertainties are only weakly dependent on altitude (Hinson, 2007; Tyler et al., 2007), which supports this assertion.

11. Effects of defocusing, critical refraction and multipath propagation

The preceding sections have discussed somewhat idealized radio occultation experiments. The phenomena of defocusing, critical refraction and multipath propagation can complicate real radio occultation experiments. These are summarized here.

Refraction can cause near-parallel rays to diverge, which reduces the signal intensity. This is called defocusing (Kursinski et al., 1997; Häusler et al., 2006). The ratio of the power of the radio beam after exiting the atmosphere to its power before entering the atmosphere is $(1 - Ld\alpha/da)^{-1}$, where L is the distance between the point of closest approach to the planet and the closest radio element (Karayel and Hinson, 1997; Kursinski et al., 2000). Using Eq. (34) and $a/H \gg 1$, this ratio is $(1 + L\alpha/H)^{-1}$ (Eshleman et al., 1980). Section 10 quantifies how the uncertainties in measured atmospheric properties depend on the strength of the radio signal. The strength of the radio signal can also be reduced by the absorption of the radio signal by atmospheric gases, such as ammonia (Lindal et al., 1981; Howard et al., 1992). Defocusing and absorption reduce the signal strength, but critical refraction can prevent the radio signal from leaving the atmosphere at all. Critical refraction occurs when the radius of curvature of the ray path is smaller than the radius of curvature of a surface of uniform refractivity (Kursinski et al., 1997). The ray path curves down towards the planetary interior, never propagating out of the atmosphere to the receiver. Critical refraction occurs when $d\mu/dr + \mu/r = 0$ or, when Eq. (28) is valid, when $v(r - H)/H = 1$ (Karayel and Hinson, 1997; Yakovlev, 2002). Defocusing, absorption and critical refraction are most significant in the deep atmospheres of Venus and the giant planets.

Multipath propagation occurs when the receiver simultaneously receives radio signals that have taken different paths through the planetary atmosphere. Formally, $\alpha(a)$ is multi-valued and ray crossing occurs. In this case, the frequency shift, Δf, observed at a given time cannot be unambiguously assigned to one closest approach distance, r, since the multiple radio signals have different tangent heights. The geometrical optics treatment of the radio occultation fails. Multipath propagation occurs when "an interval of high refractivity gradient overlies a region of lower gradient" (Kursinski et al., 1997). This is a particular problem around thin plasma layers on the bottomsides of giant planet ionospheres (Hinson et al., 1998b).

12. Discussion of results

Both σ_{Ne} and σ_{nn} are proportional to $\sigma_{\Delta f}/V \times \sqrt{H/R}$, where $H = H_p$ for the ionosphere and $H = H_n$ for the neutral atmosphere. The value of σ_{Ne} is also proportional to f. The value of σ_{nn} is also inversely proportional to $f\kappa$. Values of $\sigma_{\Delta f}$, V and f can be affected by the design of the radio occultation experiment, whereas $\sqrt{H_p/R}$, $\sqrt{H_n/R}$ and κ are planetary properties that are beyond the experimenter's control.

The uncertainty in Δf depends on many variables, including integration time, bandwidth, signal power, noise power density, oscillator stability and fluctuations in interplanetary plasma. Integration time can be increased, but at the cost of reduced vertical resolution. The smallest vertical resolution consistent with geometrical optics is the Fresnel zone diameter, which is on the order of $\sqrt{\lambda/L}$ where λ is the wavelength and L is the distance between the closest radio element and the tangent point of the ray path (Kursinski et al., 1997; Hinson et al., 1999; Kursinski et al., 2000). If the received radio signal is recorded in a closed loop system, then the bandwidth is pre-determined before the experiment and must be sufficiently wide to allow for differences between the predicted and actual frequency shifts. If the received radio signal is recorded in an open loop system, then the bandwidth can be reduced during post-processing. The bandwidth must be greater than the thermal noise and the phase noise. The experimenter can influence the signal power by choosing which of the available radio elements act as transmitters. Ground-based transmitters have much greater signal power than

space-based transmitters. The signal power of a given radio element is usually determined by the mission's communication requirements, which are beyond the control of the experimenter. The noise power density can be minimized by careful hardware design. Uncertainties from oscillator instabilities can be reduced by using a two-way experiment instead of a one-way experiment if the net effect is to replace a less stable oscillator with a more stable oscillator. The Allan Deviation of oscillators on planetary spacecraft has steadily improved over time with values at 1 s integration times of 1×10^{-10} on Mariner 4, 5×10^{-12} on Voyager, and 2×10^{-13} for Mars Global Surveyor, Cassini and Venus Express (Kliore et al., 1970; Eshleman et al., 1977; Tyler et al., 2001; Kliore et al., 2004; Häusler et al., 2006). The typical Allan Deviation of ground-based oscillators at the present day is on the order of 10^{-14} to 10^{-15} at integration times of 1s–1000 s (Dick and Wang, 1991; Howard et al., 1992; Thornton and Border, 2003; Asmar et al., 2004).

The effects of fluctuations of interplanetary plasma can be minimized by reducing the path length and increasing the distance of closest approach of the ray path to the Sun. This is a major problem for spacecraft-Earth occultations that occur near solar conjunction when the ray path between the spacecraft and Earth passes very close to the Sun. Useful measurements of planetary atmospheres are rarely obtained near solar conjunction. At these times, fluctuations in plasma density in the solar corona may be studied from their effects on radio signals (e.g. Howard et al., 1992; Bird et al., 1992, 1996). As noted in Section 7, multi-frequency measurements can effectively separate refraction in plasma and neutral gases. This technique can be used to eliminate the uncertainties caused by fluctuations in the interplanetary medium from measurements of neutral atmospheric number densities.

Speed, V, is effectively determined by the top-level mission implementation design, which is usually beyond the control of the radio occultation experimenter. That is, whether the mission consists of single or multiple spacecraft and whether each spacecraft is a flyby spacecraft, planetary orbiter, or satellite orbiter. For a single spacecraft mission, possible values of V range between about 1.5 km s^{-1} for a Titan orbiter and 25 km s^{-1} for a fast outer solar system flyby such as New Horizons. Such high speeds are rare, and $V = 5$ km s^{-1} is a reasonable default value.

Frequency, f, can be selected by the radio occultation experimenter, subject to the availability of suitable transmitting and receiving equipment in the two radio elements. Only S-band, which at downlink is typically 2.3 GHz or 13 cm, was available to the first radio occultation experiments in the 1960s (Kliore et al., 1970). X-band, which at downlink is typically 8.4 GHz or 3.6 cm, became available in the 1970s (Eshleman et al., 1977). Ka-band, which at downlink is typically 32 GHz or 0.9 cm, has been available to recent missions (Kliore et al., 2004). Higher frequencies offer more bandwidth and higher data rates for communications than lower frequencies, and are less affected by plasma in the interplanetary medium and terrestrial ionosphere, so planetary spacecraft are migrating towards Ka-band for communications systems. This transition from the long-established S-band to Ka-band has both positive and negative consequences for ionospheric occultations. Multipath effects, which more pronounced at low frequencies, are reduced (e.g. Hinson et al., 1998b; Nagy et al., 2006). If uncertainties are dominated by phase (thermal) noise, then they are two (one) orders of magnitude smaller for S-band than for Ka-band. However, this is mitigated for multi-frequency (X-band and Ka-band) occultations by the excellent characterization of noise due to interplanetary plasma that Ka-band provides.

$\sqrt{H_n/R}$ is closely related to an important metric for atmospheric escape, the ratio of a molecule's gravitational potential energy to kinetic energy at the exobase. This ratio equals the ratio of the radius of the exobase to the neutral scale height at the exobase (Strobel, 2002). $\sqrt{H_p/R}$ is not as significant. $\sqrt{H_n/R}$ equals $\sqrt{k_B TR/GMm}$, where k_B is Boltzmann's constant, T is temperature, R is planetary radius, GM is the product of the gravitational constant and the mass of the body, and m is mean molecular mass. Solar system values of $\sqrt{H_n/R}$ vary by almost one order of magnitude, as shown in Table 5. Refractive volume, κ, is typically within a factor of two of 10^{-29} m^{-3}, as shown in Table 3. Therefore variations in κ from planet to planet only modify σ_{nn} by a factor of two.

13. Case studies

To provide a concrete illustration of the results of the preceding sections, we now estimate uncertainties in ionospheric electron density and neutral number density for hypothetical radio occultations at Venus, Mars, Jupiter and Titan. Bending angle and Δf at the surface or 1 bar level are also estimated. Results are listed in Table 6. Parameters adopted for case studies at Venus, Mars, Jupiter and Titan were influenced by the Venus Express, Mars Global Surveyor, Voyager and Cassini missions, respec-

Table 5
Values of $\sqrt{H_n/R}$ for solar system atmospheres. Values were obtained as discussed in Section 12 using data from Lodders and Fegley (1998) and Strobel (2002). Surface conditions were used for solid planets and satellites; conditions at the equatorial 1-bar level were used for fluid planets.

Object	$\sqrt{H_n/R}$
Venus	0.05
Earth	0.04
Mars	0.05
Jupiter	0.02
Saturn	0.09
Titan	0.09
Uranus	0.03
Neptune	0.03
Triton	0.10
Pluto	0.13

Table 6
Representative parameters and resultant uncertainties in electron and neutral number densities for radio occultations at Venus, Mars, Jupiter and Titan.

	Venus	Mars	Jupiter	Titan
$\sigma_{\Delta f}$ (mHz)	10	10	10	10
f (GHz)	8.4[g]	8.4[k]	2.3[o]	2.3[s]
V (km s^{-1})	7.0[h]	3.4[l]	14[p]	5.6[t]
H_n (km)	7[i]	10[m]	25[q]	20[u]
H_p (km)	10[j]	25[n]	1000[r]	130[v]
R (km)[a]	6050	3400	70,000	2575
κ (m^3)[b]	1.8×10^{-29}	1.8×10^{-29}	6.2×10^{-30}	1.1×10^{-29}
α (rad)[c]	2.7×10^{-2}	1.8×10^{-4}	3.6×10^{-2}	3.6×10^{-2}
Δf (Hz)[d]	5.4×10^{3}	1.7×10^{1}	3.9×10^{3}	1.5×10^{3}
σ_{Ne} (m^{-3})[e]	1.5×10^{9}	6.3×10^{9}	5.8×10^{8}	2.7×10^{9}
σ_{nn} (m^{-3})[f]	3.8×10^{19}	1.3×10^{20}	1.1×10^{20}	7.4×10^{20}

[a] Lodders and Fegley (1998).
[b] Values of κ found using $\kappa = k_B C_1$ and C_1 from Table 4.
[c] Bending angle at the surface for Mars and Titan and at the 1 bar level for Venus and Jupiter. Values found from Eq. (34) using data from this Table and atmospheric pressure and temperature from Lodders and Fegley (1998).
[d] Frequency shift at the surface for Mars and Titan and at the 1 bar level for Venus and Jupiter. Values found from Eq. (3) using data from this Table.
[e] Values of σ_{Ne} are calculated using Eq. (38).
[f] Values of σ_{nn} are calculated using Eq. (39).
[g] X-band, Pätzold et al. (2009).
[h] Intermediate value for Venus Express orbit, also representative of 600 km circular orbit.
[i] H_n at 1 bar level, value from Tellmann et al. (2009).
[j] Pätzold et al. (2009).
[k] X-band, Tyler et al. (2001).
[l] Circular orbit around Mars at 400 km altitude.
[m] H_n at the surface, value from Lodders and Fegley (1998).
[n] Hanson et al. (1977).
[o] S-band, Hinson et al. (1998b).
[p] Circular orbit around Jupiter at the orbital distance of Europa.
[q] H_n at the 1 bar level, value from Lodders and Fegley (1998).
[r] Hinson et al. (1998b).
[s] S-band, Nagy et al. (2006).
[t] Circular orbit around Saturn at the orbital distance of Titan.
[u] H_n at the surface, value from Lodders and Fegley (1998).
[v] Kliore et al. (2008).

tively. However, thermal noise properties for Venus Express, Voyager and Cassini have not been reported in the literature. Papers on radio occultation observations usually state σ_{AD}, but rarely provide information sufficient to calculate $\sigma_{thermal}$ from Eq. (23). Hence the same value of $\sigma_{\Delta f}$, 10 mHz, was assumed in all four case studies based on the Mars Global Surveyor results of Hinson et al. (1999). This should be considered when the accuracies of the case studies are evaluated.

The estimated uncertainties at Venus are 1.5×10^9 m^3 and 3.8×10^{19} m^3 for electron density and neutral number density, respectively. Pätzold et al. (2009) reported that uncertainties in electron densities measured by Venus Express were 2×10^9 m^3, very similar to those estimated here. The smallest pressures reported by Tellmann et al. (2009) from Venus Express data were ≈1 Pa. For a temperature of 200 K, this corresponds to a neutral number density of 3×10^{20} m^3 or 1 order of magnitude greater than estimated here. Since pressure depends on the upper boundary condition used to integrate the equation of hydrostatic equilibrium, it is likely that the smallest pressure reported corresponds to an altitude one or two scale heights below the altitude of the smallest detected neutral number density. This would improve the accuracy of the predicted uncertainty.

The estimated uncertainties at Mars are 6.3×10^9 m^3 and 1.3×10^{20} m^3 for electron density and neutral number density, respectively. Mean values of Mars Global Surveyor's uncertainties are 4.6×10^9 m^{-3} for electron densities and 1.9×10^{20} m^{-3} for neutral number densities (Hinson, 2007; Tyler et al., 2007; Withers et al., 2008). The estimated uncertainties are within 50% of the mean observed uncertainties. The estimated value of Δf at the surface, 17 Hz, is several times greater than the 6 Hz value reported by Hinson et al. (1999) for one particular occultation, but is the same order of magnitude. This difference could be caused by the assumption in Eq. (3) that the frequency shift is proportional to spacecraft speed, when it is more accurate to assume that the frequency shift is proportional to the component of spacecraft velocity along the Earth-spacecraft line. This component is less than the speed. Note that this should also reduce V in Eqs. (38) and (39), which will increase σ_{Ne} and σ_{nn}.

The estimated uncertainties at Jupiter are 5.8×10^8 m^3 and 1.1×10^{20} m^3 for electron density and neutral number density, respectively. The uncertainty in Voyager electron density observations is on the order of 10^9 m^3 (Hinson et al., 1998b), consistent with the estimate. However, the smallest neutral number density reported during the Voyager 1 egress radio occultation is between 10^{22} m^3 and 10^{23} m^3 (Lindal et al., 1981). This difference of 2–3 orders of magnitude is too large to be accounted for by inappropriate choices for V, f and H. It is possible that the value of $\sigma_{\Delta f}$ appropriate for the neutral atmospheric analysis of Lindal et al. (1981) is much greater than 10 mHz, yet 10 mHz seems consistent with the later ionospheric analysis of Hinson et al. (1998b). It is possible that different bandwidths ($2B$) and integration times ($\tau_{thermal}$) were used by Lindal et al. (1981) and Hinson et al. (1998b), which would affect $\sigma_{\Delta f}$ in accordance with Eq. (23), but resolution of this discrepancy is beyond the scope of this paper.

The estimated uncertainties at Titan are 2.7×10^9 m^3 and 7.4×10^{20} m^3 for electron density and neutral number density, respectively. Uncertainties in electron density from Cassini observations are 10^8 m^3 (Kliore et al., 2008), much smaller than estimated here. Neutral atmospheric profiles from Cassini have not yet been published (Flasar et al., 2007). Since Kliore et al. (2008) noted that Δf at the ionospheric peak ($N_e \approx 10^9$ m^{-3}) at X-band is only 1 mHz, it is clear that Cassini's value of $\sigma_{\Delta f}$ is significantly smaller than the 10 mHz assumed in Table 6. Yet rearrangement of Eq. (38), use of most of the Titan-specific parameters from Table 6, replacement of $f = 2.3$ GHz (S-band) with $f = 8.4$ GHz (X-band), and assumption of an electron density of

10^9 m^{-3} (Kliore et al., 2008) yields a predicted Δf of 1 mHz—exactly the value quoted by Kliore et al. (2008). Thus the relationships derived in this work appear consistent with Kliore et al. (2008), even if the estimated uncertainties in Table 6 are too large due to incorrect assumptions about $\sigma_{\Delta f}$. It is not surprising that Cassini has a much smaller uncertainty in Δf than Mars Global Surveyor, since Cassini carries the most sophisticated planetary radio science investigation yet flown, including the first use of Ka-band signals in planetary radio occultations and averaging of results obtained using multiple frequencies and multiple ground stations (Kliore et al., 2004; Nagy et al., 2006).

14. Conclusions

We have derived theoretical relationships for uncertainties in ionospheric electron density and neutral number density in radio occultation experiments. Uncertainties in both densities are proportional to $\sigma_{\Delta f}/V \times \sqrt{H/R}$, where $H = H_p$ for the ionosphere and $H = H_n$ for the neutral atmosphere. Uncertainty in electron density is also proportional to f. Uncertainty in neutral number density is also inversely proportional to $f\kappa$. The value of $\sigma_{\Delta f}$ depends on thermal noise and phase noise. Thermal noise in past radio occultation experiments is typically hard to determine from published reports, but phase noise can be estimated from reported Allan Deviations. Lower limits on measurement uncertainties for one-way downlink radio occultation experiments can be calculated from the Allan Deviation of the spacecraft oscillator.

Predictions have been compared to data from Venus, Mars, Jupiter and Titan using a characteristic value of $\sigma_{\Delta f}$ appropriate for Mars Global Surveyor observations. Predicted and actual uncertainties in electron density agree to within 50% at Venus, but predicted uncertainties in neutral number density appear one order of magnitude too small. This large discrepancy can probably be attributed to the smallest reported pressure corresponding to an altitude some distance below that of the smallest detected neutral number density. Predicted and actual uncertainties agree to within 50% at Mars. Estimated uncertainties in ionospheric electron density at Jupiter are within 50% of observed uncertainties. Estimated uncertainties in neutral number density at Jupiter are 2–3 orders of magnitude smaller than the smallest observed neutral number density. We have not found a convincing explanation why predictions and observations are comparable at Jupiter for electron densities, but not neutral densities. Estimated uncertainties in ionospheric electron density at Titan are two orders of magnitude greater than the observed uncertainties. This depends on $\sigma_{\Delta f}$. The estimated frequency shift at Titan's ionospheric peak, which does not depend on $\sigma_{\Delta f}$, agrees almost exactly with observations. This indicates that the performance of the Cassini radio occultation investigation is excellent and its actual value of $\sigma_{\Delta f}$ is significantly smaller than the 10 mHz value assumed in this paper. It does not indicate that the method used to estimate the uncertainties is wrong.

The simple expressions developed here can be used for preliminary design studies of future radio occultation experiments. Obviously, more realistic simulations should be used for detailed design studies.

Acknowledgements

PW acknowledges productive discussions with Kerri Cahoy, Martin Pätzold, the radio science teams of Mars Express and Venus Express, and many colleagues involved in the Radio Science Experiment, led by Michael Mendillo, of "The Great Escape" mission that underwent a Phase A study for NASA's Mars Scout program. PW also thanks Bernd Häusler for a pre-publication copy of "Venus atmospheric, ionospheric, surface, and interplanetary radio wave propagation studies with the Venus Express radio science experiment VeRa", which is a VeRa instrument paper submitted for publication in a forthcoming ESA Special Publication on the Venus Express mission and payload.

References

Ahmad, B., Tyler, G.L. The two-dimensional resolution kernel associated with retrieval of ionospheric and atmospheric refractivity profiles by Abelian inversion of radio occultation phase data. Radio Sci. 33, 129–142, 1998.

Ahmad, B., Tyler, G.L. Systematic errors in atmospheric profiles obtained from Abelian inversion of radio occultation data: effects of large-scale horizontal gradients. J. Geophys. Res. 104, 3971–3992, 1999.

Allan, D.W. Statistics of atomic frequency standards. Proc. IEEE 54 (2), 221–230, 1966.

Anthes, R.A., Bernhardt, P.A., Chen, Y., Cucurull, L., Dymond, K.F., Ector, D., Healy, S.B., Ho, S.-P., Hunt, D.C., Kuo, Y.-H., Liu, H., Manning, K., McCormick, C., Meehan, T.K., Randel, W.J., Rocken, C., Schreiner, W.S., Sokolovskiy, S.V., Syndergaard, S., Thompson, D.C., Trenberth, K.E., Wee, T.-K., Yen, N.L., Zeng, Z. The COSMIC/FORMOSAT-3 mission: Early results. Bull. Am. Met. Soc. 89, 313–333, 2008.

Arfken, G.B., Weber, H.J. Mathematical Methods for Physicists, fourth ed Academic Press, San Deigo, 1995.

Ashcroft, N.W., Mermin, N.D. Solid State Physics. Holt, Rinehart and Winston, New York, 1964.

Asmar, S.W., Armstrong, J.W., Iess, L., Tortora, P. Precision of radio science instrumentation for planetary exploration. In: Third ESA International Workshop on Tracking, Telemetry and Command Systems for Space Applications, Darmstadt, Germany, 2004. Available at <http://hdl.handle.net/2014/38725>.

Bird, M.K., Asmar, S.W., Brenkle, J.P., Edenhofer, P., Pätzold, M., Volland, H. The coronal-sounding experiment. Astron. Astrophys. Suppl. 92, 425–430, 1992.

Bird, M.K., Pätzold, M., Edenhofer, P., Asmar, S.W., McElrath, T.P. Coronal radio sounding with Ulysses: Solar wind electron density near 0.1 AU during the 1995 conjunction. Astron. Astrophys. 316, 441–448, December, 1996.

Born, M., Wolf, E. Principles of Optics. Pergamon Press, London, 1959.

Bose, T.K., Cole, R.H. Dielectric and pressure virial coefficients of imperfect gases. II. CO_2–Argon mixtures. J. Chem. Phys. 52, 140–147, 1970.

Bose, T.K., Sochanski, J.S., Cole, R.H. Dielectric and pressure virial coefficients of imperfect gases. V. Octopole moments of CH_4 and CF_4. J. Chem. Phys. 57, 3592–3595, 1972.

Bracewell, R.N. The Fourier Transform and its Applications, second ed. McGraw-Hill Series in Electrical Engineering Networks and Systems, McGraw-Hill, New York, 1986.

Dick, G.J., Wang, R.T. Ultra-stable performance of the superconducting cavity maser. IEEE Trans. Instrum. Measur. 40, 174–177, 1991.

Eshleman, V.R. The radio occultation method for the study of planetary atmospheres. Planet. Space Sci. 21, 1521–1531, 1973.

Eshleman, V.R., Tyler, G.L., Anderson, J.D., Fjeldbo, G., Levy, G.S., Wood, G.E., Croft, T.A. Radio science investigations with Voyager. Space Sci. Rev. 21, 207–232, 1977.

Eshleman, V.R., Tyler, G.L., Freeman, W.T. Deep radio occultations and "evolute flashes"—their characteristics and utility for planetary studies. Icarus 37, 612–626, 1979.

Eshleman, V.R., Steffes, P.G., Muhleman, D.O., Nicholson, P.D. Comment on absorbing regions in the atmosphere of Venus as measured by radio occultation. Icarus 44, 793–803, 1980.

Essen, L. The refractive indices of water vapour, air, oxygen, nitrogen, hydrogen, deuterium and helium. Proc. Phys. Soc. B 66, 189–193, 1953.

Essen, L., Froome, K.D. The refractive indices and dielectric constants of air and its principal constituents at 24,000 Mc/s. Proc. Phys. Soc. B 64, 862–875, 1951.

Fjeldbo, G., Kliore, A.J., Eshleman, V.R. The neutral atmosphere of Venus as studied with the Mariner V radio occultation experiments. Astron. J. 76, 123–140, 1971.

Fjeldbo, G., Kliore, A., Sweetnam, D., Esposito, P., Seidel, B., Howard, T. The occultation of Mariner 10 by Mercury. Icarus 29, 439–444, 1976.

Flasar, F.M., Schinder, P.J., Marouf, E.A., French, R.G., McGhee, C.A., Kliore, A.J., Rappaport, N.J. The meridional and vertical structure of Titan's atmosphere from Cassini radio occultations. Fall Meeting of the American Geophysical Union, Abstract #P21D-02, 2007.

Gehrels, T., Matthews, M.S. Saturn. University of Arizona Press, Tucson, Arizona, 1984.

Gurnett, D.A., Kirchner, D.L., Huff, R.L., Morgan, D.D., Persoon, A.M., Averkamp, T.F., Duru, F., Nielsen, E., Safaeinili, A., Plaut, J.J., Picardi, G. Radar soundings of the ionosphere of Mars. Science 310, 1929–1933, 2005.

Hanson, W.B., Sanatani, S., Zuccaro, D.R. The Martian ionosphere as observed by the Viking retarding potential analyzers. J. Geophys. Res. 82, 4351–4363, 1977.

Häusler, B., Pätzold, M., Tyler, G.L., Simpson, R.A., Bird, M.K., Dehant, V., Barriot, J., Eidel, W., Mattei, R., Remus, S., Selle, J., Tellmann, S., Imamura, T. Radio science investigations by VeRa onboard the Venus Express spacecraft. Planet. Space Sci. 54, 1315–1335, 2006.

Hecht, E. Optics, fourth ed. Addison-Wesley, Reading, Massachusetts, 2002.

Hinson, D.P. MGS RST Science Data Products, USA_NASA_JPL_-MORS_1102. In: MGS-M-RSS-5-EDS-V1.0, MGS RST Science Data Products, USA_NASA_JPL_MORS_1102. NASA Planetary Data System, 2007.

Hinson, D.P., Flasar, F.M., Kliore, A.J., Schinder, P.J., Twicken, J.D., Herrera, R.G. Jupiter's ionosphere: Results from the first Galileo radio occultation experiment. Geophys. Res. Lett. 24, 2107–2110, 1997.

Hinson, D.P., Kliore, A.J., Flasar, F.M., Twicken, J.D., Schinder, P.J., Herrera, R.G. Galileo radio occultation measurements of Io's ionosphere and plasma wake. J. Geophys. Res. 103, 29343–29358, 1998a.

Hinson, D.P., Twicken, J.D., Karayel, E.T. Jupiter's ionosphere: New results from Voyager 2 radio occultation measurements. J. Geophys. Res. 103, 9505–9520, 1998b.

Hinson, D.P., Simpson, R.A., Twicken, J.D., Tyler, G.L., Flasar, F.M. Initial results from radio occultation measurements with Mars Global Surveyor. J. Geophys. Res. 104, 26997–27012, 1999.

Hinson, D.P., Simpson, R.A., Twicken, J.D., Tyler, G.L., Flasar, F.M. Erratum: Initial results from radio occultation measurements with Mars Global Surveyor. J. Geophys. Res. 105, 1717–1718, 2000.

Howard, H.T., Eshleman, V.R., Hinson, D.P., Kliore, A.J., Lindal, G.F., Woo, R., Bird, M.K., Volland, H., Edenhoffer, P., Pätzold, M. Galileo radio science investigations. Space Sci. Rev. 60, 565–590, 1992.

Imamura, T., Iwata, T., Yamamoto, Z., Oyama, K.-I., Nabatov, A., Kono, Y., Matsumoto, M., Liu, Q., Noda, H., Hanada, H., Futaana, Y., Saito, A. Initial results of the lunar ionosphere observation with SELENE radio science. Lunar and Planetary Science Conference, vol. 39, Abstract 1659, 2008a.

Imamura, T., Oyama, K.-I., Iwata, T., Kono, Y., Matsumoto, K., Liu, Q., Noda, H., Futaana, Y., Nabatov, A. The possibility of studying the lunar ionosphere with the SELENE radio science experiment. Earth, Planets, Space 60, 387–390, 2008b.

Karayel, E.T., Hinson, D.P. Sub-Fresnel-scale vertical resolution in atmospheric profiles from radio occultation. Radio Sci. 32, 411–424, 1997.

Kliore, A.J. Satellite atmospheres and magnetospheres. Highlights Astron. 11, 1065–1069, 1998.

Kliore, A., Cain, D.L., Siedel, B.L., Fjeldbo, G. S-band occultation for Mariner Mars 1971. Icarus 12, 82–90, 1970.

Kliore, A.J., Fjeldbo, G., Seidel, B.L., Sweetnam, D.N., Sesplaukis, T.T., Woiceshyn, P.M., Rasool, S.I. The atmosphere of Io from Pioneer 10 radio occultation measurements. Icarus 24, 407–410, 1975.

Kliore, A.J., Hinson, D.P., Flasar, F.M., Nagy, A.F., Cravens, T.E. The ionosphere of Europa from Galileo radio occultations. Science 277, 355–358, 1997.

Kliore, A.J., Herrera, R.G., Hinson, D.P., Twicken, J.D., Flasar, F.M., Schinder, P.D. The ionosphere of Io and the plasma environments of Europa, Ganymede, and Callisto. American Astronomical Society's Division for Planetary Sciences Meeting, Abstract 55.09, 1998.

Kliore, A.J., Anabtawi, A., Herrera, R.G., Asmar, S.W., Nagy, A.F., Hinson, D.P., Flasar, F.M. Ionosphere of Callisto from Galileo radio occultation observations. J. Geophys. Res. 107, 1407, doi:10.1029/2002JA009365, 2002.

Kliore, A.J., Anderson, J.D., Armstrong, J.W., Asmar, S.W., Hamilton, C.L., Rappaport, N.J., Wahlquist, H.D., Ambrosini, R., Flasar, F.M., French, R.G., Iess, L., Marouf, E.A., Nagy, A.F. Cassini Radio Science. Space Sci. Rev. 115, 1–70, 2004.

Kliore, A.J., Nagy, A.F., Marouf, E.A., French, R.G., Flasar, F.M., Rappaport, N.J., Anabttawi, A., Asmar, S.W., Kahann, D.S., Barbinis, E., Goltz, G.L., Fleischman, D.U., Rochblatt, D.J. First results from the Cassini radio occultations of the Titan ionosphere. J. Geophys. Res. 113, A09317, doi:10.1029/2007JA012965, 2008.

Kołos, W., Wolniewicz, L. Polarizability of the hydrogen molecule. J. Chem. Phys. 46, 1426–1432, 1967.

Kursinski, E.R. The GPS radio occultation concept: Theoretical performance and initial results. Ph.D. thesis, California Institute of Technology, 1997.

Kursinski, E.R., Hajj, G.A., Schofield, J.T., Linfield, R.P., Hardy, K.R. Observing Earth's atmosphere with radio occultation measurements using the Global Positioning System. J. Geophys. Res. 102, 23429–23465, 1997.

Kursinski, E.R., Hajj, G.-A., Leroy, S.S., Herman, B. The GPS radio occultation technique. Terr. Atmos. Ocean. Sci. 11, 53–114, 2000.

Lide, D.R. CRC Handbook of Chemistry and Physics, 75th ed. CRC Press, Boca Raton, Florida, 1994.

Lindal, G.F. The atmosphere of Neptune—An analysis of radio occultation data acquired with Voyager 2. Astron. J. 103, 967–982, 1992.

Lindal, G.F., Wood, G.E., Levy, G.S., Anderson, J.D., Sweetnam, D.N., Hotz, H.B., Buckles, B.J., Holmes, D.P., Doms, P.E., Eshleman, V.R., Tyler, G.L., Croft, T.A. The atmosphere of Jupiter—An analysis of the Voyager radio occultation measurements. J. Geophys. Res. 86, 8721–8727, 1981.

Lindal, G.F., Lyons, J.R., Sweetnam, D.N., Eshleman, V.R., Hinson, D.P. The atmosphere of Uranus—Results of radio occultation measurements with Voyager 2. J. Geophys. Res. 92, 14987–15001, 1987.

Lindsey, W.C. Synchronization Systems in Communication and Control. McGraw-Hill, New York, 1972.

Lipa, B., Tyler, G.L. Statistical and computational uncertainties in atmospheric profiles from radio occultation—Mariner 10 at Venus. Icarus 39, 192–208, 1979.

Lodders, K., Fegley, B. The Planetary Scientist's Companion. Oxford University Press, New York, 1998.

Maccone, C., Pluchino, S. Studying the lunar ionosphere by virtue of the SMART-1 signals. Memorie della Societa Astron. Italiana Suppl. 11, 63–67, 2007.

Mendillo, M., Smith, S., Wroten, J., Rishbeth, H., Hinson, D. Simultaneous ionospheric variability on Earth and Mars. J. Geophys. Res. 108, 1432, doi:10.1029/2003JA009961, 2003.

Möller, K.D. Optics. University Science Books, Mill Valley, California, 1988.

Nagy, A.F., Kliore, A.J., Marouf, E., French, R., Flasar, M., Rappaport, N.J., Anabtawi, A., Asmar, S.W., Johnston, D., Barbinis, E., Goltz, G., Fleischman, D. First results from the ionospheric radio occultations of Saturn by the Cassini spacecraft. J. Geophys. Res. 111, A06310, doi:10.1029/2005JA011519, 2006.

Niemann, H.B., Atreya, S.K., Bauer, S.J., Carignan, G.R., Demick, J.E., Frost, R.L., Gautier, D., Haberman, J.A., Harpold, D.N., Hunten, D.M., Israel, G., Lunine, J.I., Kasprzak, W.T., Owen, T.C., Paulkovich, M., Raulin, F., Raaen, E., Way, S.H. The abundances of constituents of Titan's atmosphere from the GCMS instrument on the Huygens probe. Nature 438, 779–784, 2005.

Orcutt, R.H., Cole, R.H. Dielectric constants of imperfect gases. III. Atomic gases, hydrogen and nitrogen. J. Chem. Phys. 46, 697–702, 1967.

Pätzold, M., Neubauer, F.M., Andreev, V.E., Gavrik, A.L. Detection of the inner plasma pileup region at Comet Halley during the Vega 1 flyby by the radio sounding experiment. J. Geophys. Res. 102, 2213–2222, 1997.

Pätzold, M., Neubauer, F.M., Carone, L., Hagermann, A., Stanzel, C., Häusler, B., Remus, S., Selle, J., Hagl, D., Hinson, D.P., Simpson, R.A., Tyler, G.L., Asmar, S.W., Axford, W.I., Hagfors, T., Barriot, J.-P., Cerisier, J.-C., Imamura, T., Oyama, K.-I., Janle, P., Kirchengast, G., Dehant, V. MaRS: Mars Express Orbiter Radio Science. ESA SP-1240: Mars Express: the Scientific Payload, pp. 141–163, 2004. Available at <http://sci.esa.int/science-e/www/object/index.cfm?fobjectid=34885>.

Pätzold, M., Tellmann, S., Häusler, B., Hinson, D., Schaa, R., Tyler, G.L. A sporadic third layer in the ionosphere of Mars. Science 310, 837–839, 2005.

Pätzold, M., Tellmann, S., Häusler, B., Bird, M.K., Tyler, G.L., Christou, A.A., Withers, P. A sporadic layer in the Venus lower ionosphere of meteoric origin. Geophys. Res. Lett. 36, L05203, doi:10.1029/2008GL035875, 2009.

Phinney, R.A., Anderson, D.L. On the radio occultation method for studying planetary atmospheres. J. Geophys. Res. 73, 1819–1827, 1968.

Pluchino, S., Schilliro, F., Cassaro, P. First results from the ionospheric radio occultations of the Moon by spacecraft. European Planetary Science Congress, Abstract EPSC2007-A-00206, 2007.

Rappaport, N., Bertotti, B., Giampieri, G., Anderson, J.D. Doppler measurements of the quadrupole moments of Titan. Icarus 126, 313–323, 1997.

Reinisch, B.W., Haines, D.M., Bibl, K., Cheney, G., Galkin, I.A., Huang, X., Myers, S.H., Sales, G.S., Benson, R.F., Fung, S.F., Green, J.L., Boardsen, S., Taylor, W.W.L., Bougeret, J.-L., Manning, R., Meyer-Vernet, N., Moncuquet, M., Carpenter, D.L., Gallagher, D.L., Reiff, P. The radio plasma imager investigation on the IMAGE spacecraft. Space Sci. Rev. 91, 319–359, 2000.

Rishbeth, H., Garriott, O.K. Introduction to Ionospheric Physics. Academic Press, New York, 1969.

Robinson, F.N.H. Macroscopic Electromagnetism. Pergamon Press, Oxford, 1973.

Rocken, C., Kuo, Y.-H., Schreiner, W., Hunt, D., Sokolovskiy, S., McCormick, C. COSMIC system description. Terr. Atmos. Ocean. Sci. 11, 21–52, 2000.

Schunk, R.W., Nagy, A.F. Ionospheres. Cambridge Univ. Press, New York, 2000.

Simon, M.K., Yuen, J.H. Receiver design and performance characteristics, in: Yuen, J.H. (Ed.), Deep Space Telecommunications Systems Engineering. Plenum Press, New York, pp. 49–121, 1983.

Sniffin, R.W. DSN telecommunications link design handbook. NASA JPL DSN 810-005, Rev. E, 2001. Available at <http://eis.jpl.nasa.gov/deepspace/dsndocs/810-005/>.

Stern, S.A. The lunar atmosphere: History, status, current problems, and context. Rev. Geophys. 37, 453–491, 1999.

Strobel, D.F. Aeronomic systems on planets, moons, and comets. In: Mendillo, M., Nagy, A.F., Waite, J.H. (Eds.), Atmospheres in the Solar System: Comparative Aeronomy, Geophys. Monogr. Ser. American Geophysical Union, vol. 130, Washington, DC, pp. 7–22, 2002.

Tellmann, S., Pätzold, M., Häusler, B., Bird, M.K., Tyler, G.L. Structure of the Venus neutral atmosphere as observed by the radio science experiment VeRa on Venus Express. J. Geophys. Res. 114, E00B36, doi:10.1029/2008JE003204, 2009.

Thornton, C.L., Border, J.S. Radiometric tracking techniques for deep-space navigation. Wiley-Interscience, Hoboken, New Jersey, 2003. Available at <http://descanso.jpl.nasa.gov/Monograph/mono.cfm>.

Tyler, G.L., Howard, H.T. Refractivity of carbon dioxide under simulated Martian conditions. Radio Sci. 4, 899–904, 1969.

Tyler, G.L., Sweetnam, D.N., Anderson, J.D., Borutzki, S.E., Campbell, J.K., Kursinski, E.R., Levy, G.S., Lindal, G.F., Lyons, J.R., Wood, G.E. Voyager radio science observations of Neptune and Triton. Science 246, 1466–1473, 1989.

Tyler, G.L., Balmino, G., Hinson, D.P., Sjogren, W.L., Smith, D.E., Simpson, R.A., Asmar, S.W., Priest, P., Twicken, J.D. Radio science observations with Mars Global Surveyor: Orbit insertion through one Mars year in mapping orbit. J. Geophys. Res. 106, 23327–23348, 2001.

Tyler, G.L., Balmino, G., Hinson, D.P., Sjogren, W.L., Smith, D.E., Woo, R.W., Armstrong, J.W., Flasar, F.M., Simpson, R.A., Asmar, S., Anabtawi, A., Priest, P. MGS RST Science Data Products, USA_-NASA_JPL_MORS_1038. In: MGS-M-RSS-5-SDP-V1.0, MGS RST Science Data Products, USA_NASA_JPL_MORS_1038. NASA Planetary Data System, 2007.

Tyler, G.L., Linscott, I.R., Bird, M.K., Hinson, D.P., Strobel, D.F., Pätzold, M., Summers, M.E., Sivaramakrishnan, K. The New Horizons Radio Science Experiment (REX). Space Sci. Rev. 140, 217–259, 2008.

Withers, P. A review of observed variability in the dayside ionosphere of Mars. Adv. Space Res. 44, 277–307, 2009.

Withers, P., Towner, M.C., Hathi, B., Zarnecki, J.C. Analysis of entry accelerometer data: A case study of Mars Pathfinder. Planet. Space Sci. 51, 541–561, 2003.

Withers, P., Mendillo, M., Hinson, D.P., Cahoy, K. Physical characteristics and occurrence rates of meteoric plasma layers detected in the Martian ionosphere by the Mars Global Surveyor Radio Science Experiment. J. Geophys. Res. 113, A12314, doi:10.1029/2008JA013636, 2008.

Wu, X., Hu, X., Gong, X., Zhang, X., Wang, X. Analysis of inversion errors of ionospheric radio occultation. GPS Solut. 13, 231–239, 2009.

Yakovlev, O.I. Space Radio Science. Taylor and Francis, New York, 2002.

Yelle, R.V., Miller, S. Jupiter's thermosphere and ionosphere, in: Bagenal, F., Dowling, T.E., McKinnon, W.B. (Eds.), Jupiter: The Planet, Satellites, and Magnetosphere. Cambridge University Press, New York, pp. 185–218, 2004.